ACS OMEGA

Open Access

http://pubs.acs.org/journal/acsodf

Article

Deep Eutectic Solvents as Designer Phase-Change Materials for Organic Rankine Cycle Applications

Published as part of ACS Omega special issue "Energy Storage across Scales".

Johan González, Pía Cruz, Ricardo Hernández, Fèlix Llovell, José Matías Garrido, and Héctor Quinteros-Lama*

Cite This: ACS Omega 2026, 11, 22031−22043

Read Online

ACCESS | Metrics & More | Article Recommendations | Supporting Information

ABSTRACT: Organic Rankine cycles (ORCs) are one of the most prominent technologies for efficient energy use, from renewable or residual energy sources. These systems are widely used due to their simple design and flexibility. One interesting addition to an ORC is a thermal energy accumulator (TEA), which can improve the energy utilization efficiency. This contribution analyzes the thermal and exergetic efficiency changes when a TEA is added to an ORC. Seven novel deep eutectic solvent (DES)-based phase-change materials (PCMs) are studied and compared with paraffin wax used as a benchmark compound. The ORC uses ten different working fluids (WF), including fluorinated gases and hydrocarbons (HCs). The results show that R1233zd and *n*-pentane are the working fluids reaching the highest thermal and exergetic efficiency, while choline chloride plus suberic acid and choline chloride plus 4-hydroxybenzoic acid are the best PCMs, far exceeding the exergetic performance of paraffin wax. Furthermore, adding a TEA improves the quality of energy delivery, increasing the exergetic efficiency by up to 95%. These findings highlight the practicality of using hydrocarbons in ORCs in conjunction with TEAs. Additionally, the analysis indicates that PCMs with a higher-melting-temperature and fusion enthalpy offer the most promising solution for ORCs with TEAs, thereby providing valuable insights for the design and optimization of ORC systems.

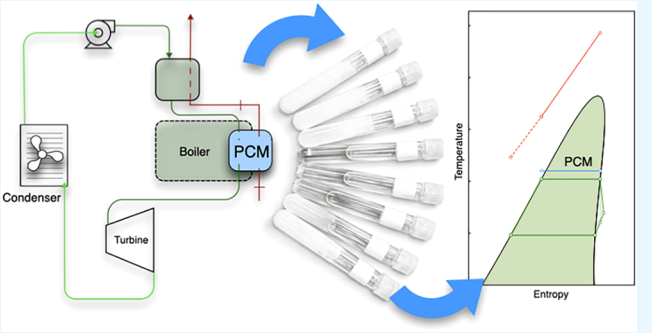

INTRODUCTION

Efficient energy utilization is one of the ways to combat excessive carbon dioxide (CO_2) production. CO_2 constitutes the most significant amount of greenhouse gas produced by anthropogenic sources and is one of the leading agents of climate change, principally produced by fossil fuels associated with growing global energy demand. Enhancing energy efficiency and reducing these energy needs is widely considered to be the most promising, fastest, cheapest, and safest way to mitigate climate change associated with CO_2.[1]

Organic Rankine cycles (ORCs) are systems characterized by efficient energy use, given their simple design and control, lower maintenance, reliability, and great flexibility.[2,3] Notably, this flexibility is a desirable characteristic combined with other technologies to improve its energy efficiency.[4−12]

Traditionally, ORC efficiency was improved by increasing the temperature of the energy source to achieve higher vapor pressure in the working fluids (WF), based on the Carnot principle.[13,14] Another usual way to increase efficiency is by selecting a working fluid from a previously chosen set of suitable compounds to maximize the thermal efficiency or net output work.[2,15,16] These approaches utilize limit conditions, such as the temperature of the energy sources and the heat sink. Although less common, the working fluid selection can also be based on achieving the maximum exergetic efficiency in the system.[5,6,8,17,18] The previously cited literature contributions provided criteria for the correct selection of working fluids, where the most commonly preferred fluids are R113, R134a, R227, R236ea, R236fa, and R245fa. However, these compounds must be obliterated by 2030 due to their high Global Warming Potential (GWP), as mandated by the different national and international regulations, principally the Kigali Agreement.[19−21] For this reason, there is growing interest in finding alternative replacements.

Hydrocarbons (HCs) have always been evaluated as possible working fluids in ORCs, given their zero ozone-depleting potential (ODP) and very low GWP.[22] Consequently, many

Received: December 16, 2025
Revised: March 26, 2026
Accepted: March 30, 2026
Published: April 1, 2026

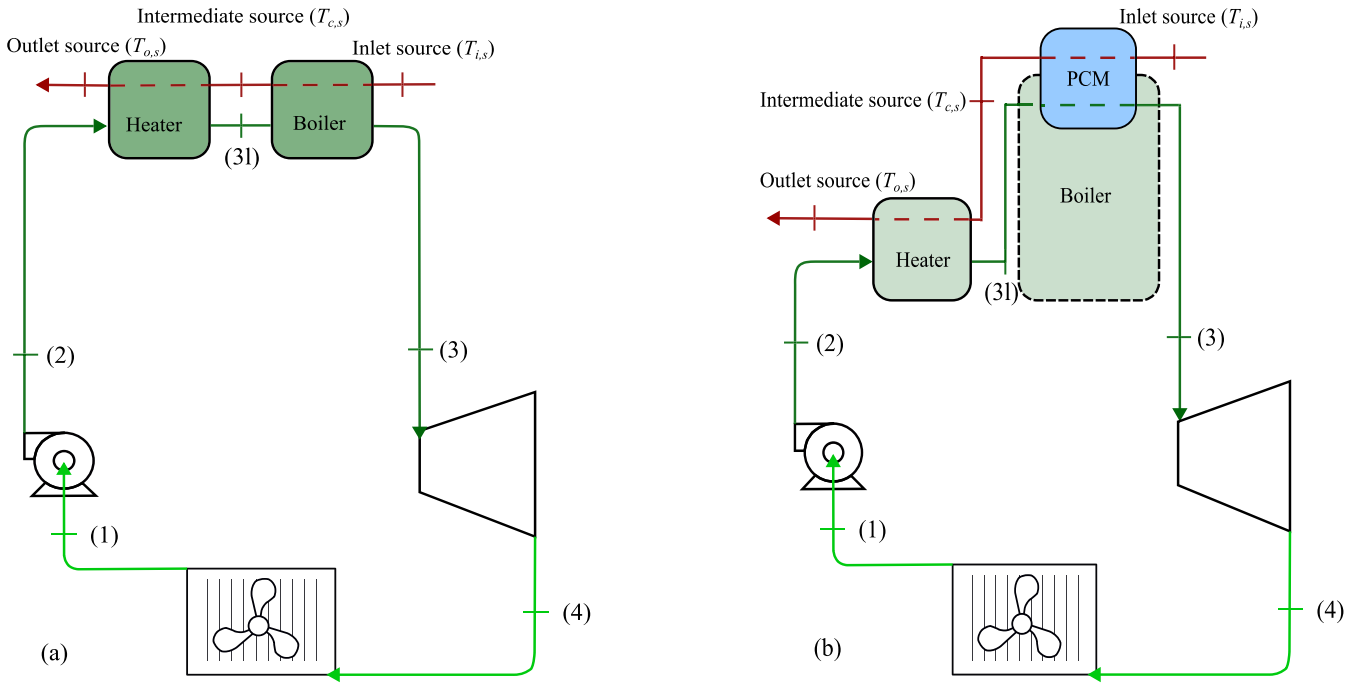

Figure 1. A schematic representation of an organic Rankine cycle composed of a pump, a heater or heat exchanger, a turbine, and a condenser. (a) The organic Rankine cycle is thermally powered by exhaust gases as an energy source. (b) The organic Rankine cycle is thermally powered by an energy accumulator fed by exhaust gases as an energy source.

research studies on improving their efficiency have been carried out.[2,6,9,23,24] Similarly, hydrofluoroolefins (HFOs), commonly called fourth-generation refrigerants, have also been analyzed in the pursuit of an adequate replacement for traditional fluorinated working fluids. Fourth-generation refrigerants are anthropogenic working fluids with zero ODP and low GWP.[25−27] These refrigerants are outlined as promising on the near horizon due to their thermal efficiency, low exergy production, and net power output.[17,28−32] However, despite having suitable thermophysical properties, most HFOs are flammable. Consequently, their use as single compounds may be limited.[33]

Apart from a proper selection of the working fluid, other improvements related to the increase of the thermal or exergetic efficiency in ORCs include the addition of heat exchanger units, such as heat recuperators, economizers, and thermal oil accumulators.[2,6,8,16,34−36] However, a recent innovative approach to increase the efficiency and reduce exergy destruction and intermittency of some nonconventional renewable energy sources is the use of thermal energy accumulators (TEAs) with phase-change materials (PMCs).[6,10,12,37]

PCMs are compounds capable of absorbing heat when the material undergoes a phase transition, usually by melting, which is later released upon crystallization or solidification. Paraffin waxes are the most commonly used compounds.[38−40] However, the use of waxes in ORCs is limited by their properties, such as the melting point, enthalpy of fusion, and viscosity. Dragomir-Stanciu and Luca[37] showed that it is possible to produce electricity through an ORC that uses paraffin wax as a PCM in a TEA, albeit on a small scale due to the large amount of paraffin required.

The search for alternative PCMs includes fatty acids, high-molecular-weight hydrocarbons, salts, ionic liquids, and deep eutectic solvents (DESs).[41−47] Indeed, several authors evaluated the use of these potential compounds. For example, Daniarta et al.[42] examined an ORC within the framework of Carnot batteries aimed at storing electrical energy as thermal energy in TEAs. This work evaluated critical parameters for selecting the working fluid and the PCM that optimize operational conditions. Regarding the analysis of PCMs, two materials were selected based on their high-melting enthalpies and low mass flow requirements for thermal energy supply. Notably, barium hydroxide octahydrate and acetamide emerged as standout candidates. In another contribution, Matuszek et al.[48] presented some ionic liquids based on guanidinium to be used as TEAs. The results showed the importance of the concentration and strength of the hydrogen bonds in the enthalpy of fusion of PCMs. They also reported an appropriate set of ionic liquids with a melting-temperature range between 100 and 220 °C, which can potentially be used in ORCs as TEAs.

In recent years, DESs have taken the leading role in the past decade to the detriment of ionic liquids.[49,50] The interest in DESs lies in their easy synthesis and low cost,[51,52] while keeping similar equilibrium and transport properties (i.e., density, viscosity, refractive index, conductivity, surface tension, and chemical inertness) to those of traditional ionic liquids.[53] In particular, their low pressure, flammability, and tunability are desirable characteristics for use in TEAs.[10] Choline chloride-based DESs as hydrogen-bond acceptors (HBA) were utilized as TEAs. Indeed, a pioneering contribution from Peyrovedin et al.[10] revealed that a combination of choline chloride (ChCl) with 4-hydroxybenzoic acid at a molar ratio of 1:0.5 provided better results than paraffin waxes from an energetic and exergetic point of view, delivering 25% more net power output, with a decrease in the amount of PCM required in the operation of a solar ORC. PCMs enable compact storage of large energy quantities, with studies showing that salt hydrates, such as $MgCl_2{\cdot}6H_2O$, can

https://doi.org/10.1021/acsomega.5c13210
ACS Omega 2026, 11, 22031−22043

maximize system efficiency, while KNO_2-NaNO_3 and acetamide contribute to peak ORC and collector efficiencies.[54] In direct vapor generation systems, where the working fluid is vaporized within the solar collectors, annual system efficiency and net power output improve by 71.96 and 64.38%, respectively, compared to indirect configurations.[55] TEA integration into ORC components, such as evaporators and heaters, has also been optimized using dimensionless storage mass parameters, providing design guidelines for efficient PCM-based systems.[45] Moreover, enhancing PCM thermal conductivity with metal foams has been shown to significantly increase stored energy, highlighting the role of advanced materials in improving ORC-TEA performance.[56]

This work is devoted to analyzing the exergetic efficiency of a source composed of seven PCMs based on DESs, plus paraffin wax, which serves as a benchmark for thermal accumulator materials. These PCMs are combined with ten pure refrigerants as working fluids. The thermal efficiency of a coupled ORC is evaluated, demonstrating the independence of this parameter from the thermal storage system. Two exergetic analyses are carried out: the first corresponds to the exergetic efficiency between the thermal source and the working fluid and the second to the exergetic efficiency between the PCMs and the working fluid. The effect of varying the pinch-point temperatures is assessed in both cases. The improvement in exergetic efficiency, combined with the easy tunability of DES-based PCMs, represents the primary advantage of using these systems as thermal accumulators, which can be designed depending on the working fluid and optimal operating conditions. The above highlights their ability to adapt to the system's operating conditions and the characteristics of the working fluid. Therefore, the study of PCMs, with thermophysical properties tailored for a working fluid and characteristics of the available thermal source, is an uncharted territory that can significantly improve the characteristics of these systems, enabling their practical use across multiple scales.

THEORY AND MODELING

Figure 1a illustrates a basic ORC driven by a thermal energy source. The ORC system consists of a pump, a heater or heat exchanger, a boiler, a vapor turbine, and a condenser. As is customary, saturated vapor at state point (3) expands in the turbine, generating mechanical work at point (4). Subsequently, isobaric condensation occurs at state point (1). The saturated liquid is then pressurized by the pump (2), heated (3l), and vaporized again, reaching state point (3). The ideal isentropic expansion is depicted by the dotted line terminating at point (4r). Figure 1b displays the same layout connected to a direct TEA, where a thermal source feeds the accumulator and the PCM transfers the heat to the working fluid. For this case, Figure 2 shows the temperature profile of the thermal source in crimson. The latter profile shows three fundamental points for analyzing the source.

The ORC system was kept as simple as possible, assuming reversible processes in the turbomachinery, in order to isolate the effects of the ORC layout on the changes induced in the TEA system. Additionally, it is important to highlight that the isentropic efficiencies of the turbine and pump have no impact on the performance of the thermal source; they affect only the thermal efficiency of the cycle, which can be considered a separate matter.

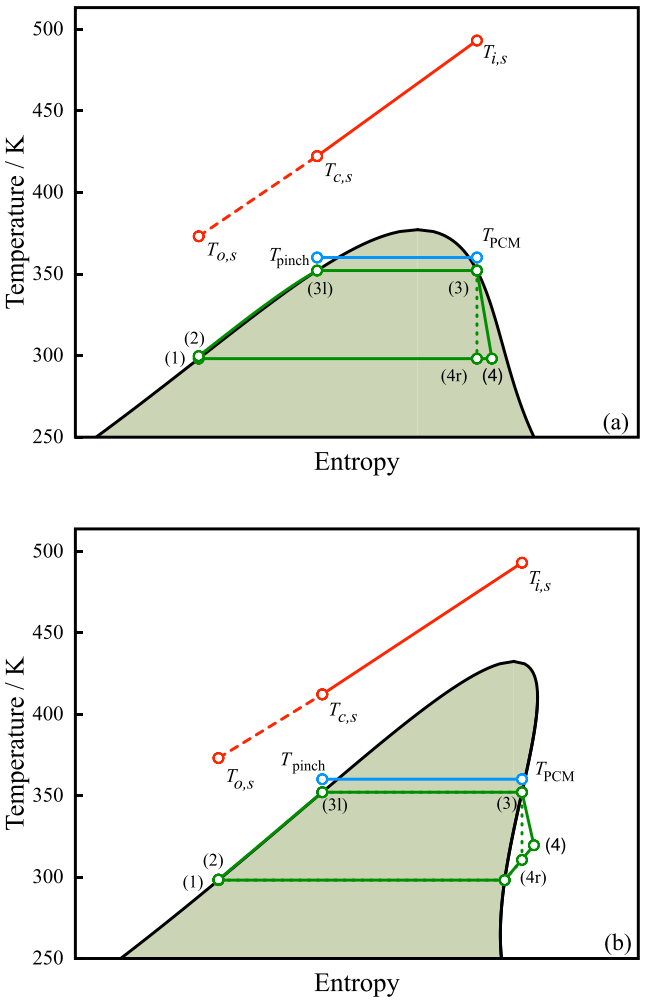

Figure 2. Schematic illustrations of an ORC, including a TEA, in the temperature vs entropy projection. Illustrations also depict the thermal source and PMC temperature profiles. (a) R22, a working fluid with a wet expansion. (b) *n*-Butane displaying a dry expansion. In both cases, $T_{i,s}$, $T_{c,s}$, and $T_{o,s}$ are the inlet (i), intermediate (c), and outlet (o) temperatures of the thermal source, respectively.

The thermal source enters the TEA with temperature $T_{i,s}$. At the end of the process and after transferring the heat to the TEA, the temperature of the thermal source is $T_{c,s}$. The remaining energy of the thermal source is directly delivered to the working fluid for preheating the saturated liquid at point (2−3l). After both transfer processes, the outlet temperature of the thermal source is $T_{o,s}$.

The TEA temperature profile is rendered in blue, assuming that the process has no sensible effects. Therefore, the two end points of the blue line are at the same temperature, T_{PCM}, and represent the temperature of the phase change of the PCM, located between the thermal source and the boiler temperature. Further, Figure 2 also illustrates the temperature gap between the TEA and saturation temperatures of the working fluid, ensuring good heat transfer. This temperature is termed the pinch-point temperature, T_{pinch}. The three temperature profiles have different entropy scales depending on the material. Consequently, the line positions in the horizontal axis are merely illustrative.

It is a widely known fact that the thermal efficiency of a power cycle, η_I, is determined by the ratio of the net work, W_n, to the energy used in the process, Q. In a single-stage ORC,

https://doi.org/10.1021/acsomega.5c13210
ACS Omega 2026, 11, 22031−22043

where each piece of equipment has the same mass flow, the thermal efficiency, η_I, is given by

$$\eta_I = \frac{W_n}{Q} \tag{1}$$

where $W_n = \dot{W}_n/\dot{m}$ and $Q = \dot{Q}/\dot{m}$, being $\dot{m}$ the mass flow in the ORC. The added heat is the sum of the amount of energy of the heater (h) and the boiler (b), $\dot{Q} = \dot{Q}_h + \dot{Q}_b$. Additionally, the net work may be written as $\dot{W}_n = \dot{Q} - \dot{Q}_c$, with $\dot{Q}_c$ being the amount of extracted heat in the condenser (c).

All of the amount of heat can be expressed as enthalpy differences. For instance, the energy of the heater is given by

$$\dot{Q}_h = \dot{m}(\tilde{H}_{3l} - \tilde{H}_2) = -\dot{m}_s(\tilde{H}_{o,s} - \tilde{H}_{c,s}) \tag{2}$$

while the energy of the boiler yields

$$\dot{Q}_b = \dot{m}(\tilde{H}_3 - \tilde{H}_{3l}) = -\dot{m}_s(\tilde{H}_{c,s} - \tilde{H}_{i,s}) \tag{3}$$

where $\tilde{H}_i$ is the molar enthalpy of the ith flow rate, following the same nomenclature of the ORC lines in Figures 1 and 2, i.e., $\tilde{H}_1$ concerns the enthalpy of the saturated liquid leaving the condenser.

Now, considering an exergy approach, the flow-specific exergy[57] can be defined as

$$\psi_i = \tilde{H}_i - \tilde{H}_0 - T_0(\tilde{S}_i - \tilde{S}_0) \tag{4}$$

where the subscript i concerns the flow, while the subscript 0 represents the dead-point condition, chosen at a temperature of reference equal to 293.15 K.

In an adiabatic heat exchanger system composed of two flows, the exergy supplied is a decrease in the hot-flow exergy. In contrast, the exergy recovered is the increase in the cold-flow exergy, as long as it is not at a lower temperature than the surroundings.[10,57] Therefore, in a directly energized ORC, such as that of Figure 1a, the exergetic efficiency, η_{II}, of the boiler and the source in contact with the boiler (sb) is the ratio between the received exergy and the dispensed exergy by the source. Hence, it can be obtained as

$$\eta_{II,b} = \eta_{II,sb} = -\frac{\dot{m}(\psi_3 - \psi_{3l})}{\dot{m}_s(\psi_{c,s} - \psi_{i,s})} \tag{5}$$

In contrast, when the TEA is included, the exergetic efficiencies of the boiler and the source are not the same because direct contact is lost. Therefore, the exergetic efficiency of the boiler in contact with the PCM is given by

$$\eta_{II,b} = \eta_{II,TEA} = -\frac{\dot{m}(\psi_3 - \psi_{3l})}{\dot{m}_{PCM}(\psi_{o,PCM} - \psi_{i,PCM})} \tag{6}$$

The numerical subscripts refer to the ORC flows, while b and s denote the boiler and thermal source, respectively. TEA and PMC represent the thermal accumulator exergetic efficiency and the phase-change material flow. The PCM is presented as a mass flow. However, it is easy to scale to a mass amount considering that $m_{PCM} = \dot{m}_{PCM}t_R = \dot{m}_s C_{P,s}\Delta T_s\ t_R/\Delta\tilde{H}_{f,PCM}$, where t_R is the residence time of the source in the TEA heat exchanger.

In the previous formulation, the differences on the PCM exergies depend on the PCM melting enthalpy, $\Delta\tilde{H}_{f,PCM}$, and temperature, T_m, following

$$\psi_{o,PCM} - \psi_{i,PCM} = \Delta\tilde{H}_{f,PCM}\left(1 - \frac{T_0}{T_m}\right) \tag{7}$$

where $\Delta\tilde{H}_{f,PCM}$ is the PCM melting enthalpy at a fixed concentration while T_0 and T_m is the dead-point and melting temperatures, respectively.

All calculations performed in this work are based on the simplest ORC with a mass flow of 1 kg s^{-1} of working fluid. The above is because the configuration of the ORC does not impact the exergetic efficiency of the PCM, but only the thermal efficiency. The system is considered to be in steady-state conditions for all cycle components, and heat and friction losses are neglected. The boiler has been analyzed in a temperature range between 312.15 and 361.15 K, while the condenser temperature was fixed at 298.15 K. Moreover, the driving equipment is isentropic, i.e., their efficiency is 100%. In any case, the efficiency of the turbomachinery does not influence the exergetic evaluation of the isobaric stages as it is only relevant to the thermal efficiency of the cycle. Nevertheless, assuming that the mechanical work of the pump is negligible, the nonideal thermal efficiency of the cycle can be obtained by multiplying the ideal thermal efficiency by the average isentropic efficiency of the turbine. The thermal source is a combustion exhaust gas, modeled using the standard air assumptions and data.[58] The inlet and outlet air temperatures are fixed at 493.15 and 373.15 K, respectively. The mass flow ratio of the thermal source varies depending on the energy needed by the working fluid to reach the saturated vapor state. Additionally, three discrete values for the pitch point temperature are considered in typical operation ranges (5, 8, and 11 K). All numerical assumptions delimiting the scope of this study are summarized in Table 1. It is essential to emphasize that thermal efficiency is not influenced by the manner in which energy is delivered to the system but by only the amount of energy. In contrast, the exergetic efficiency is impacted by the trajectory of the energy.

Table 1. Input Parameters and Boundary Conditions for ORC Thermally Powered by a Thermal Energy Accumulator

	value	range
	organic Rankine cycle	
working fluid mass flow	1.0 kg s^{-1}	
heat exchanger temperature		312.15−361.15 K
condenser temperature	298.15 K	
expander isentropic efficiency	1.0	
pump isentropic efficiency	1.0	
	energy source and TEA	
exhaust gases temperature		493.15−373.15 K
pinch-point temperature		5, 8, and 11 K

The calculation of the air enthalpy and entropy is done through a second-order polynomial fitted to render the air data

$$\tilde{H}_{air} = \alpha_{1,0} + \alpha_{1,1}T + \alpha_{1,2}T^2 + \tilde{H}_r \tag{8}$$

and

$$\tilde{S}_{air} = \alpha_{2,0} + \alpha_{1,1}T + \alpha_{1,2}T^2 + \tilde{S}_r \tag{9}$$

where subscripts r, in enthalpy and entropy, concern an arbitrary reference state and the constants of eqs 8 and 9 are presented in Table 2.

https://doi.org/10.1021/acsomega.5c13210
ACS Omega 2026, 11, 22031−22043

Table 2. Constants for the Air Enthalpy, eq 8, and Entropy, eq 9

i	$\alpha_{i,1}$	$\alpha_{i,2}$	$\alpha_{i,3}$
1	kJ kg^{-1}	kJ kg^{-1} K^{-1}	kJ kg^{-1} K^{-2}
	5.8341	$9.6110\cdot10^{-1}$	$6.6642\cdot10^{-5}$
2	kJ kg^{-1} K^{-1}	kJ kg^{-1} K^{-2}	kJ kg^{-1} K^{-3}
	0.4713	$4.9931\cdot10^{-3}$	$-2.9897\cdot10^{-6}$

Seven DES-based PCMs were analyzed along with paraffin wax as a benchmark. DES-based PCM offers environmental advantages over paraffin waxes, particularly at the beginning and end of their life cycles. Paraffin waxes come from petroleum products with poor biodegradability and significant toxicity in their final disposal.[59] In contrast, DESs are based on choline chloride (ChCl) as the hydrogen-bond acceptor (HBA), which is the most common constituent. ChCl is inexpensive, nontoxic, and readily available, even in large amounts, for industrial uses.[10,41,49,50,53,60−63] ChCl is combined with urea and six carboxylic acids, acting as hydrogen-bond donors (HBDs). On the one hand, urea is extremely cheap, nontoxic, and available. On the other hand, carboxylic acids form DES with strong hydrogen bonding and, hence, exhibit a wide range of equilibrium temperatures, which can be tailored to the working fluids for exergetic optimization. The selected carboxylic acids are, in general, low-hazard compounds in this application, although they may cause irritation to the skin and eyes upon direct contact. In some cases, respiratory irritation was also been reported. However, the vapor pressures of these compounds are negligible, which significantly limits the risk of inhalation exposure. Further details regarding the safety characteristics of these compounds are provided in the Supporting Information.

Additionally, all of the selected DESs have available data with similar melting temperatures and have been used as PCMs.[10] Table 3 shows the designation of each PCM, including their HBDs, molar ratio, molecular weight, melting temperature, and enthalpy of fusion of the HBD, PCM, and paraffin wax. The enthalpy of fusion of the PCM can be calculated as an ideal solution, as

$$\Delta\tilde{H}_{f,PCM} = z_{HBD}\Delta\tilde{H}_{f,HBD} + z_{HBA}\Delta\tilde{H}_{f,HBA} \quad (10)$$

where z_{HBD} and z_{HBA} are the molar fractions of the HBD and HBA, respectively. The mixing enthalpy is ignored for DES because the dimensionless excess Gibbs energy function is considered to uniquely depend on the concentration, as in the case of activity coefficients models. As a consequence, the excess and mixing enthalpies are null.

Different families of compounds were selected as working fluids. R22 and R134a are chosen because of their outstanding technical properties, being the most commonly used hydrochlorofluorocarbons (HCFC) and hydrofluorocarbons (HFC), respectively.[66,67] Despite the ban on R22, this refrigerant is still used in big refrigeration systems in some countries and is one of the most common refrigerants that require replacement. Isobutane, *n*-butane, isopentane, and *n*-pentane are also included as HCs that stand out for their promising performance in ORCs[28,29,57] due to their null-GWP. However, their high flammability may limit their applicability as working fluids in large-scale systems.[68] Additionally, R1234yf, R1243zf, R1234ze, and R1233zd are fourth-generation refrigerants, usually utilized as a replacement for traditional HFC and HCFC to overcome GWP problem,[4,30,31,69] despite the fact that they are associated with other environmental concerns.[70] The main safety properties are described in the Supporting Information. The thermophysical properties of the ten working fluids are modeled using the PC-SAFT equation of state (EOS).[71] The aforementioned EOS is a molecular-based approach capable of accurately predicting the required properties of the ORC modeling. The model has been widely used in the modeling of working fluids and ORC.[72−75] The details of the PC-SAFT approach can be found in the original contribution, and a brief description is provided in the Supporting Information. The assumptions for the modeling with PC-SAFT can be found in the previous contribution on the limiting efficiency of an ORC.[73] Table 4 shows the molecular parameters of each working fluid for the PC-SAFT EOS.

RESULTS AND DISCUSSION

Thermal Efficiency

Figure 3a−c depicts the thermal efficiency of the ten working fluids in combination with the seven DES-based PCM and paraffin. The heat of fusion of the PCM drives the energy requirements of the ORC. Therefore, each PCM is limited to a maximum thermal efficiency, η_I, at the temperature of fusion of the material. The layouts are analyzed at pinch temperatures, T_{pinch}, of 5, 8, and 11 K between the boiler and the TEA. In all cases, as well as the pinch-point temperature increases, the overall efficiency of the studied combinations decreases. Regardless of the pinch-point temperatures, the highest thermal efficiency is achieved by PCM1, followed by those by PCM4 and PCM2. In contrast, PCM6, PCM7, and paraffin reach the lowest thermal efficiencies. This fact is directly related to the PCM fusion temperature since the efficiency is strongly correlated with this value.[23,28]

Table 3. Choline Chloride as HBA and a Set of HBD at Different Molar Ratios[a]

PCM	HBD	HBA:HBD molar	$M_{w,PCM}$ (g mol^{-1})	$\Delta\tilde{H}_{f,PCM}$ (kJ mol^{-1})	$\Delta\tilde{H}_{f,PCM}$ (J g^{-1})	T_m (K)	references
PCM1	suberic acid	1.0:1.0	156.92	30.23	192.65	366.15	64,65
PCM2	urea	1.0:0.9	102.22	22.17	216.89	353.15	61,64
PCM3	gallic acid	1.0:0.5	149.79	30.17	201.42	350.15	64,65
PCM4	hydroxybenzoic acid	1.0:0.5	139.13	30.50	219.22	360.15	64,65
PCM5	oxalic acid	1.0:0.8	117.81	22.08	187.42	346.15	61,64
PCM6	itaconic acid	1.0:1.0	134.87	23.62	175.13	330.15	64,65
PCM7	*p*-coumaric acid	1.0:0.5	147.81	23.10	190.11	340.15	64,65
paraffin					189.00	341.15	41

$\Delta\tilde{H}_{f,HBA}$ = 29.76 kJ mol^{-1}.[10]

[a]For each combination, the enthalpies of fusion and melting temperatures of each PCMs are displayed.

https://doi.org/10.1021/acsomega.5c13210
ACS Omega 2026, 11, 22031−22043

Table 4. PC-SAFT Molecular Parameters of ORC Working Fluids

compound	ASHRAE code	m	σ (Å)	ε/k_B (K)	$\bar{\nu}^L$ dev. (pph)	source
chlorodifluoromethane	R22	2.4744	3.1331	189.03	0.80	76
1,1,1,2-tetrafluoroethane	R134a	3.2483	3.0157	170.60	0.95	76
isobutane	R600a	2.2012	3.7933	219.71	0.38	28
n-butane	R600	2.3316	3.7086	222.88	1.59	71
isopentane	R601a	2.5620	3.8296	230.75	1.53	71
n-pentane	R601	2.6896	3.7729	231.20	0.78	71
HFO-1234yf	R1234yf	2.8978	3.3648	174.91	1.70	77
HFO-1243zf	R1243zf	2.7112	3.3960	186.08	0.75	78
HFO-1234ze-E	R1234ze(E)	3.2268	3.1909	173.87	0.60	78
HCFO-1233zd-E	R1233zd(E)	3.1368	3.3909	202.51	2.84	78

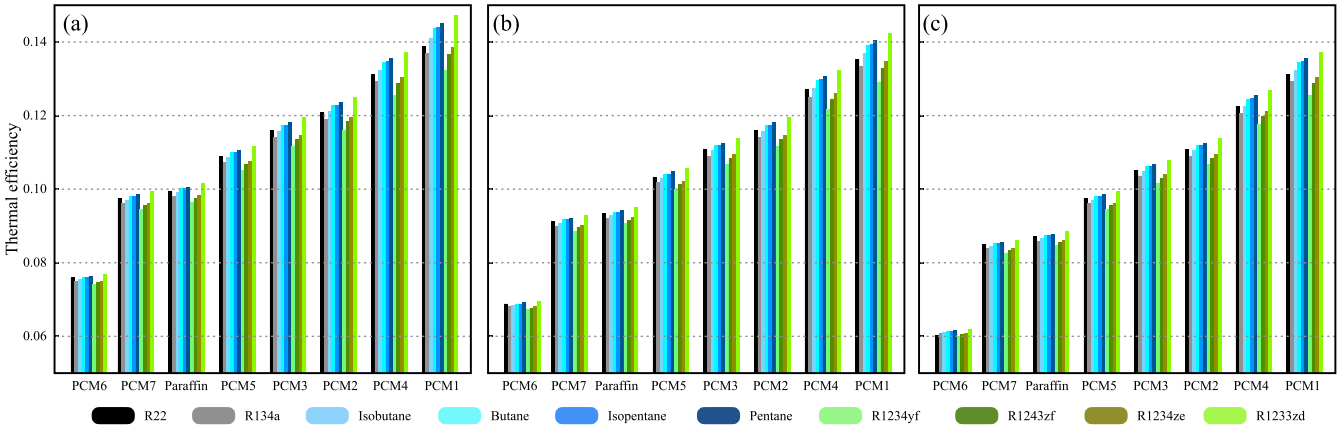

Figure 3. Thermal efficiency obtained by the ten working fluids related to adding PCMs based on DESs for their use in TEAs for a pinch-point temperature of (a) T_{pinch} = 5.00 K, (b) T_{pinch} = 8.00 K, and (c) T_{pinch} = 11.00 K.

Concerning the impact of the working fluids, it is interesting to note the significant difference in the performance of the studied HFOs, R1233zd, and R1234yf. While the combination of R1233zd with all PCMs provides the highest thermal efficiency values, using R1234yf gives one of the lowest performances. The use of hydrocarbons as working fluids also results in high thermal efficiencies, following the order pentane, butane, isopentane, and isobutane, being only surpassed by R1233zd. Finally, the use of R134a tends to give lower efficiencies, while R22 provides intermediate values. It is evident that for the same compound family the critical temperature is the most significant variable in increasing the thermal efficiency of the system. For high-melting-temperature PCMs, the differences between the thermal efficiencies of the working fluids rise for the same material. The latter reveals that the working fluid selection becomes more significant in combination with high-temperature PCMs.

Exergetic Analysis

The exergetic efficiency, η_{II}, achieved by the system is depicted in Figure 4, considering the working fluid and PCM properties. Figure 4a–c represents a direct-heated system, while Figure 4d–f includes the addition of a TEA. As done for the thermal efficiency, the discrete pinch-point temperatures are 5, 8, and 11 K.

In all cases, the exergetic efficiency increases with the temperature of phase change and decreases with the expansion of the pinch point. Hence, a higher-melting-temperature yields a conservation in energy quality and an improvement in energy reception by the working fluid. PCM1, PCM4, and PCM2, in this order, stand out with the best exergetic efficiency. Notably, the hierarchy of thermal and exergetic efficiencies is the same.

Apart from this common trend, some important differences must be noted. In Figure 4a–c, representing a classical ORC, where the exhaust gases are in contact with the working fluid, the exergetic efficiency may reach a maximum of 0.52 in the best case scenario, values consistent with those found in analogous systems in the literature.[79] The working fluids with higher efficiencies for all pinch-point temperatures are *n*-pentane and R1233zd. In contrast, the lowest values are found for R1234yf, R134a, and R1243zf. As previously observed, the changes in efficiency among the working fluids are more notorious as the pinch point increases. In contrast, the addition of a TEA increases the exergy efficiency up to 0.94 in the best case and makes the exergetic efficiency independent of the working fluid. This can be seen in Figure 4d–f, where the values are uniquely dependent on the PCM and the pinch-point temperature.

Selecting the best combination of a working fluid and a PCM involves critical variables, including not only the thermophysical characteristics of the working fluid and the PCM but also the cycle design variables. Figure 5 depicts the exergetic efficiency of the PCMs as the pinch-point temperature gap increases with respect to the refrigerant saturation temperature. For instance, for PCM1 at 340.00 K, the pinch-point temperature is given by $T_{pinch} = T_{m,PCM1} - 340.00$ K = 26.15 K. As expected from the results of Figure 5, the exergetic efficiency of the TEA-boiler system is monotonously reduced as the pinch-point temperature grows. The comparison among PCMs reveals that the correct selection of the compound may

https://doi.org/10.1021/acsomega.5c13210
ACS Omega 2026, 11, 22031−22043

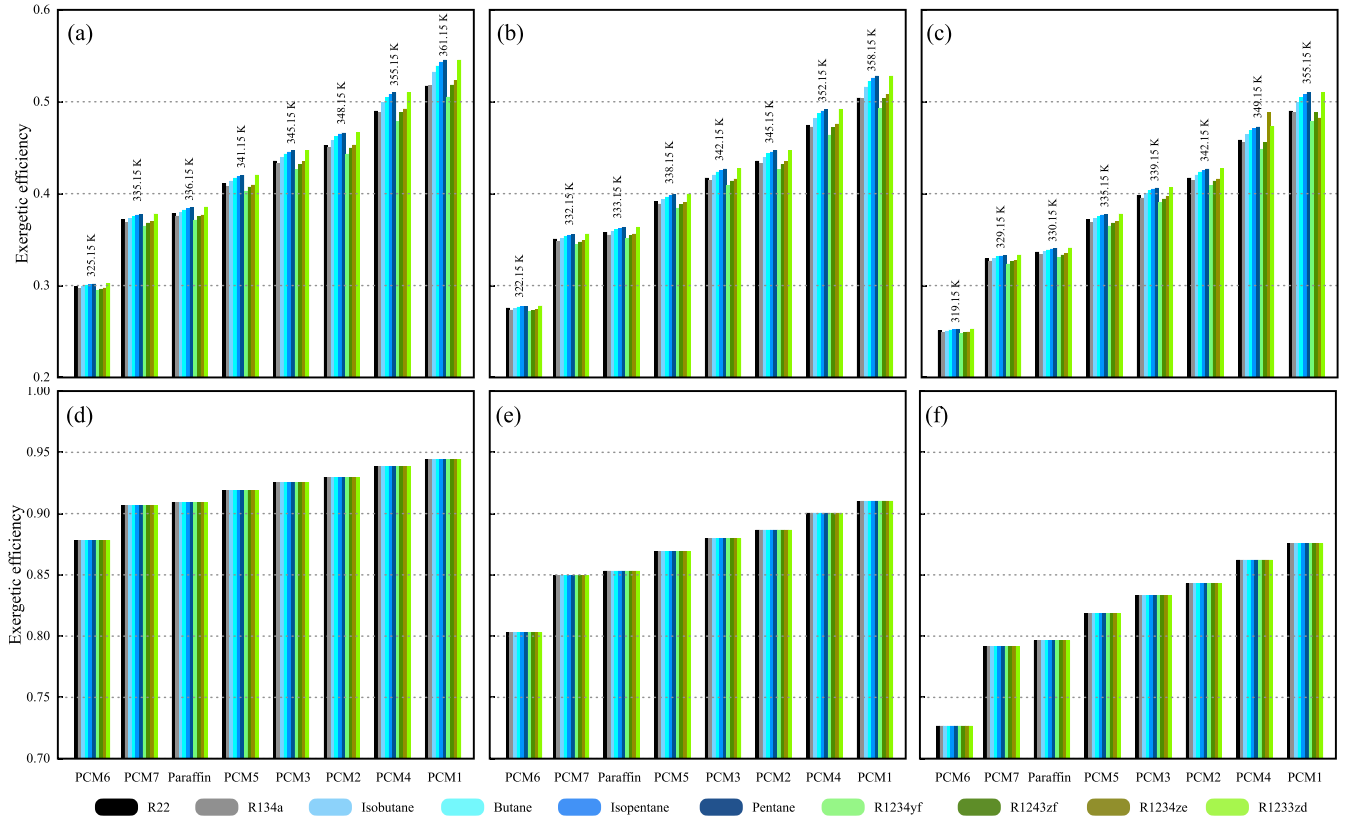

Figure 4. Exergetic efficiency obtained by the ten (10) working fluids related to adding PCMs based on DESs for their use in TEAs for several pinch-point temperatures. (a, d) Pinch-point temperature equal to 5 K. (b, e) Pinch-point temperature equal to 8 K. (c, f) Pinch-point temperature equal to 11 K.

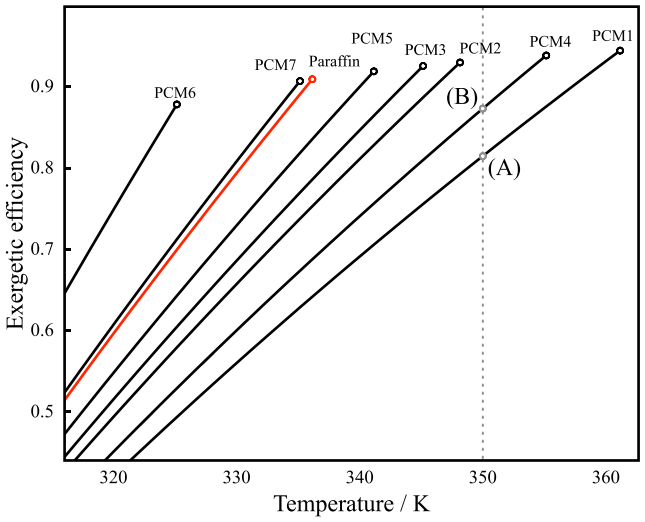

Figure 5. PCM exergetic efficiency comparison at different pinch-point temperatures. The points that crown each line have a 5 K difference compared with the melting temperature of the material.

avoid the limitations imposed by the melting temperatures of the material.

The results of the energy and exergy analyses suggest that PCM1 is the best option for the system. However, if the system were operated at a pressure with a saturation temperature of 350.00 K, as marked in the gray-dotted line in Figure 5, a greater pinch-point temperature would be required for PCM1 compared, for instance, to PCM4. This would result in a lower exergetic efficiency (point (A)), compared to PCM4 (point (B)). In that particular case, the other PCMs lie in ranges beyond the phase-change condition. Therefore, a general conclusion is that the PCM phase-change temperature is always desired to be near the saturation temperature of the working fluids at the boiler temperature.

The flow ratio between PCM and the working fluid is also a critical variable. In particular, the PCM mass flow impacts all of the design variables of the system due to the energy required to move the material, the size of the TEA, the layout of the system, and the design of the heat exchangers, to name a few. Figure 6 shows the mass flow ratio between the PCM and the working fluid, $\dot{m}_{PCM}/\dot{m}_{WF}$, to supply the required energy to reach the saturation temperature at the boiler pressure. The horizontal axis displays the pinch-point temperature difference. Figure 6a depicts the behavior of PCMs with *n*-pentane. In this case, PMC6 requires the highest mass flow for this working fluid, while PCM4, PCM2, and PCM1 require the smallest one. In the above analysis, the melting temperature of each PCM is also a variable to consider. Mainly, with a larger melting-point temperature of the phase-change material, the ORC is capable of reaching a more elevated saturation temperature in the isobaric hight-pressure stage. In the aforementioned condition, a smaller amount of energy is required for the phase change of the PCM. Therefore, a smaller PCM flow is necessary for the labor. Furthermore, as demonstrated previously, a significant improvement in exergetic efficiency may be observed at elevated pressures. For R1233zd, the results are shown in Figure 6b, displaying similar trends. Table 5 summarizes the functional average of

https://doi.org/10.1021/acsomega.5c13210
ACS Omega 2026, 11, 22031−22043

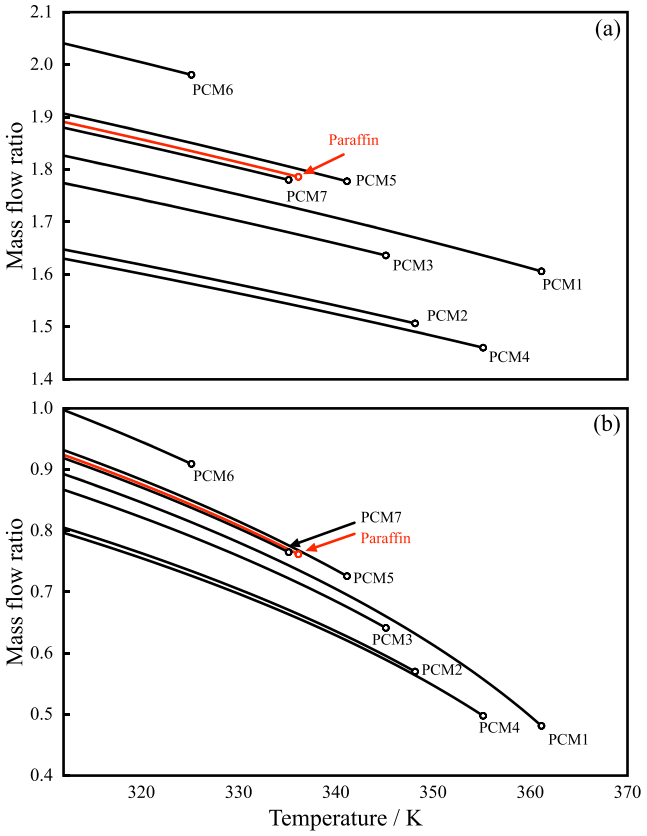

Figure 6. Mass flow ratio of the PCMs based on the DESs used as TEAs as a function of the saturation temperature of the working fluids in the heat exchanger. (a) *n*-Pentane. (b) R1233zd.

the mass flows of each PCM and working fluid between 312.00 K and the PCM melting temperature plus the minimal pinch point.

In some scenarios, it may be desirable to increase the flow ratio to avoid solidification of the PCM. However, a larger flow yields an increment in exergy destruction compared to an analogous system working without a TEA. In that case, the addition of a TEA would not provide any improvement in terms of efficiency. This limit has been quantified in Figure 7, where the PCM mass flow ratio increment to equate the exergetic efficiency of a system without a TEA has been plotted. In this example, *n*-pentane is chosen as the working fluid. In addition, Table 6 quantifies the percentage average difference between the mass flow ratio required to drive the ORC and the maximum flow ratio to avoid exergy destruction, which is given by

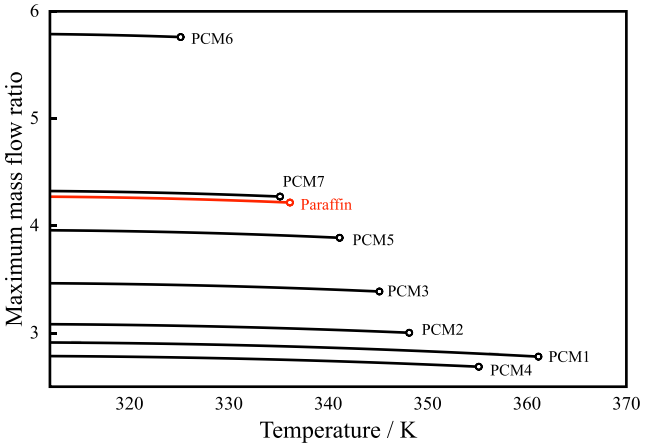

Figure 7. Maximum mass flow ratio of the PCMs based on the DESs used as TEAs as a function of the saturation temperature of the working fluids in the ORC. *n*-Pentane.

$$\Delta\dot{m} = 100\frac{\dot{m}_{\mathrm{max,PCM}} - \dot{m}_{\mathrm{PCM}}}{\dot{m}_{\mathrm{PCM}}} \tag{11}$$

where $\dot{m}_{\mathrm{max,PCM}}$ is the limiting exergetic mass flow ratio, as represented in Figure 7, and $\dot{m}_{\mathrm{PCM}}$ is the required mass flow ratio, dependent on the working fluid and the pinch-point temperature.

As can be seen in Table 6, PCM6, which was the worst material in terms of energy and exergy efficiency, has the larger flexibility to regulate the flow of the PCM. However, other highly efficient PCMs exhibit a lower operation range. This occurs because the heat transfer is performed at a higher pressure, reducing the margin of operation.

One of the well-known advantages of DESs is their tunability, which allows them to easily modify their thermophysical properties. The straightforward way to do this is by adjusting the proportion of their constituents. Among these properties, the melting temperature is the most intuitive to modify. Given the impact of this property on the thermal and exergetic efficiency of a TEA system, the PCMs can be optimized using this parameter with the knowledge of the working fluid properties.

Figure 8a displays the exergetic efficiency as a function of the temperature for a TEA system using PCM2 and *n*-pentane as the working fluid. The crimson line depicts the baseline case, where the choline chloride concentration in the DES is x_1 = 0.474. As observed, an increase in the amount of choline chloride automatically decreases the melting point, while the contrary effect occurs when the amount of urea is increased. The gray dashed line indicates a temperature of 330.00 K for

Table 5. Functional Average of the Mass Flow Ratios of Each PCM and Working Fluid between 312.00 K and the PCM Melting Temperature Plus the Minimal Pinch Point

	R22	R134a	R600a	R600	R601a	R601	R1234yf	R1243zf	R1234ze	R1233zd
PCM1	0.7186	0.7245	1.4504	1.6422	1.6155	1.7211	0.5552	0.7477	0.7075	0.8837
PCM2	0.6507	0.6552	1.3091	1.4819	1.4576	1.5528	0.5032	0.6758	0.6392	0.7973
PCM3	0.7015	0.7060	1.4099	1.5959	1.5696	1.6721	0.5425	0.7282	0.6886	0.8587
PCM4	0.6424	0.6473	1.2948	1.4658	1.4419	1.5361	0.4965	0.6679	0.6318	0.7887
PCM5	0.7549	0.7595	1.5157	1.7154	1.6870	1.7971	0.5840	0.7832	0.7405	0.9229
PCM6	0.8133	0.8163	1.6240	1.8374	1.8061	1.9242	0.6296	0.8412	0.7941	0.9883
PCM7	0.7460	0.7500	1.4949	1.6915	1.6633	1.7720	0.5773	0.7732	0.7307	0.9098
paraffin	0.7500	0.7542	1.5037	1.7015	1.6731	1.7822	0.5805	0.7776	0.7349	0.9154

https://doi.org/10.1021/acsomega.5c13210
ACS Omega 2026, 11, 22031−22043

Table 6. Percentage Difference between the Mass Flow Ratios of the Exergetic Efficiency with the Addition of PCM and the Exergetic Efficiency with the Thermal Energy Source, $\Gamma = 100(\eta_{II,air} - \eta_{II,PCM})/\eta_{II,PCM}$

	R22	R134a	R600a	R600	R601a	R601	R1234yf	R1243zf	R1234ze	R1233zd
						pph				
PCM1	69	70	68	67	67	66	72	71	70	66
PCM2	95	97	95	94	93	93	99	97	96	93
PCM3	103	105	103	102	101	101	106	105	104	101
PCM4	80	81	79	78	78	77	83	82	81	77
PCM5	115	116	115	114	113	113	118	117	116	113
PCM6	188	190	188	187	187	187	191	190	189	186
PCM7	136	138	137	135	135	135	140	138	138	134
paraffin	132	134	133	131	131	131	136	134	134	130

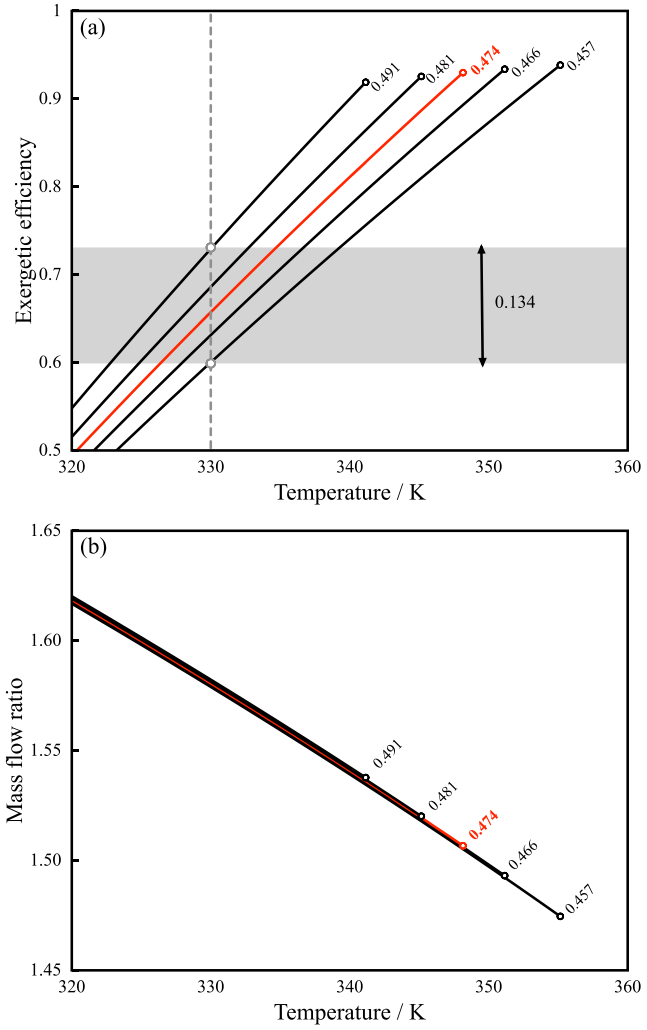

Figure 8. Response of the PCM2/*n*-pentane TEA-ORC system to the change in the concentration of the constituents of the PCM. The crimson line represents the baseline shown in the previous analysis at $x_{urea} = 0.474$, while higher-melting-temperature lines are urea-enriched systems ($x_1 = 0.457$ and $x_1 = 0.466$) and lower melting-temperature lines are choline chloride-enriched systems ($x_1 = 0.481$ and $x_1 = 0.491$). (a) Exergetic efficiency. (b) Mass flow ratio.

illustrative purposes. At this value, a dramatic increase in the exergetic efficiency is obtained by slightly enriching the urea quantity. However, the range of operation of the boiler is reduced because of the pressure limitations in the isobaric stage. Consequently, smaller mechanical work is produced, and the possibility of condensation in the turbomachinery becomes an incipient problem. In the case where higher temperatures are needed, a previous analysis regarding the eutectic line of the PCM must be carried out to avoid the formation of a solid phase.

Furthermore, the required mass flow of PCM to energize the ORC system is shown in Figure 8b. The concentration yields almost identical results. For the aforementioned reason, only the melting temperature limits the equilibrium properties concerning the mass flow. Nevertheless, other properties come into play, such as the viscosity, which influenced the design of the heat exchanger pieces of equipment. Remarkably, the scalability of the system must be almost linear as ORC energy requirements increase.

Including the concentration of PCM constituents in the optimization procedure introduces many additional variables. As mentioned before, the density, viscosity, phase-change heat, and precipitation dynamics are added to the melting temperature, underscoring the importance of the mechanical design of the TEA system. Nevertheless, tuning the ratio of DES precursors enables high tunability of DESs when used as PCMs, providing a wide range of operating temperatures and opportunities for system optimization.

CONCLUDING REMARKS

This work has analyzed the capacity of choline chloride-based deep eutectic solvents to serve as PCMs in a TEA-coupled single-stage ORC, using the PC-SAFT molecular-based equation of state. The study proposed seven different DESs and paraffin as the benchmark. The thermal and exergetic efficiencies, as well as the PCM mass flow ratio, were evaluated using a selection of ten working fluids, including HFCs, HCs, and HFOs.

The analysis demonstrates that adding a TEA improves the quality of the energy delivery, increasing the exergetic efficiency by up to 95%. On the one hand, the observed increase can be attributed to PCMs' ability to maintain the working fluid's temperature in the boiler during the phase-change stage. On the other hand, using DES as PCM offers the advantage of its tailor-made nature. As a consequence, the melting temperature can be adjusted according to the optimal conditions of the working fluid. The PCMs that achieved the highest thermal and exergetic efficiencies were PCM1 (choline chloride plus suberic acid), PCM4 (choline chloride plus 4-hydroxybenzoic acid), and PCM2 (choline chloride plus urea), all of which exceeded the exergetic efficiency of traditional paraffin wax. Overall, the efficiency was highly correlated with the PCM melting point, whose temperature should be as close as possible to the saturation temperature of the working fluid in the ORC. Among the studied working fluids, R1233zd and

https://doi.org/10.1021/acsomega.5c13210
ACS Omega 2026, 11, 22031−22043

n-pentane stood out as those with the highest thermal and exergetic efficiency, regardless of the PCM used. These fluids surpassed other common alternatives, such as R134a and R1234yf. The mass flow ratio indicated that PCM4, PCM2, and PCM1 had the lowest values, requiring a minimal flow to deliver the required energy for operation. The above is a consequence of their higher fusion enthalpy compared to other PCMs. An absolute ranking of the best PCM cannot be established due to the dependence on the working fluid and the characteristics of the available waste heat source. However, PCM1 performs best for medium-temperature applications, whereas PCM6 is better suited for low-temperature applications from an exergetic perspective.

Furthermore, the mass flow ratio is crucial for determining the flexibility of the ORC-TEA systems. Therefore, based on the thermodynamic analysis, PCM4 (choline chloride: 4-hydroxybenzoic acid) and PCM1 (choline chloride: suberic acid), in combination with *n*-pentane as the working fluid, are the most efficient pairs for an ORC-TEA system. Finally, variations in the concentrations of the PCM precursors significantly affect the behavior and design variables of the system. In the analyzed PCM, higher urea concentrations increase the exergetic efficiency under the same ORC operational conditions. However, it reduces the capability of the isobaric high-pressure stage. The above demonstrates the high tunability of DESs when used as PCMs, providing a wide range of possible operating temperatures and opportunities for system optimization.

This analysis provides a robust guideline for screening and identifying an optimal combination of PCM and working fluid to enhance the performance of power cycle layouts in scenarios requiring an energy accumulator. It identifies the main variables to consider in the study and design of an ORC with a TEA using a tunable PCM. Nonetheless, it is essential to consider other variables, such as environmental impact and flammability, when making a final recommendation.

■ ASSOCIATED CONTENT

Supporting Information

The Supporting Information is available free of charge at https://pubs.acs.org/doi/10.1021/acsomega.5c13210.

Description of the PC-SAFT model, including the parameter sets and the constants for the polynomial correlation of the isobaric heat capacity of the involved ORC working fluids, and the safety information for the DES precursors and working fluids (PDF)

■ AUTHOR INFORMATION

Corresponding Author

Héctor Quinteros-Lama − *Departamento de Tecnologías Industriales, Faculty of Engineering, Universidad de Talca, Curicó 3340000, Chile;* orcid.org/0000-0001-8953-6140; Email: hquinteros@me.com

Authors

Johan González − *Departamento de Tecnologías Industriales, Faculty of Engineering, Universidad de Talca, Curicó 3340000, Chile;* orcid.org/0000-0001-8740-8743

Pía Cruz − *Departamento de Tecnologías Industriales, Faculty of Engineering, Universidad de Talca, Curicó 3340000, Chile*

Ricardo Hernández − *Departamento de Tecnologías Industriales, Faculty of Engineering, Universidad de Talca, Curicó 3340000, Chile*

Fèlix Llovell − *Department of Chemical Engineering, ETSEQ, Universitat Rovira i Virgili, 43007 Tarragona, Spain;* orcid.org/0000-0001-7109-6810

José Matías Garrido − *Departamento de Ingeniería Química, Faculty of Engineering, Universidad de Concepción, Concepción 4070386, Chile;* orcid.org/0000-0001-9989-7206

Complete contact information is available at: https://pubs.acs.org/10.1021/acsomega.5c13210

Notes

The authors declare no competing financial interest.

■ ACKNOWLEDGMENTS

J.G., H.Q.-L., and J.M.G. acknowledge funding from ANID FONDECYT, Chile (Grant Nos. 11250144, 1240765, and 1230236, respectively). F.L. is grateful for the supported by projects REFCICLA (PID2023-149713OB-I00) and NEW-F-TECH (TED2021-130959B-I00) funded by the Spanish Ministry of Science and Innovation MCIN/AEI/10.13039/501100011033/and the European Union NextGenerationEU/PRTR.

■ NOMENCLATURE

List of Symbols

C_P	isobaric heat capacity of the perfect gas
$\tilde{H}_i$	enthalpy at point *i*
$\dot{m}$	mass flow
M_w	molar weight
Q	heat of the isobaric equipment
Q_b	added heat in the boiler
Q_c	heat in the condenser
Q_h	added heat in the heater
$\tilde{S}_i$	entropy at point *i*
T_i	thermodynamic temperature at point *i*
T_0	dead-point temperature
T_{PCM}	temperature of the phase change of the PCM
T_m	melting temperature
T_{pinch}	refers to the pinch-point temperature
t	time
W	thermodynamic work
W_n	net work

Subscripts and Superscripts

air	refers to the air
b	refers to the boiler
c	refers to the condenser
c	refers to the intermediate point of the thermal source
h	refers to the heater
i	refers to the inlet of the thermal source or PCM
l	saturate liquid
o	refers to the outlet of the thermal source or PCM
0	dead-point condition
R	residence time
r	reversible process
r	arbitrary reference state
s	refers to the thermal source
z	molar fraction of the HBA or HBD

https://doi.org/10.1021/acsomega.5c13210
ACS Omega 2026, 11, 22031−22043

Greek Letters

$\alpha_{1,i}$ constant for the enthalpy of the air
$\alpha_{2,i}$ constant for the entropy of the air
η_{I} thermal efficiency
η_{II} exergetic efficiency
ψ_i flow-specific exergy at point i

Abbreviations

DES deep eutectic solvent
EOS equation of state
GWP global warming potential
HBA hydrogen-bond acceptor
HBD hydrogen-bond donor
HC hydrocarbon
HCFC hydrochlorofluorocarbons
HFC hydrofluorocarbons
HFO hydrofluoroolefin
ODP ozone-depleting potential
ORC organic rankine cycle
PCM phase-change material
TEA thermal energy accumulator
WF working fluid

REFERENCES

(1) Sorrell, S. Reducing energy demand: A review of issues, challenges and approaches. *Renewable Sustainable Energy Rev.* **2015**, *47*, 74−82.
(2) Goyal, A.; Sherwani, A. F.; Tiwari, D. Optimization of cyclic parameters for ORC system using response surface methodology (RSM). *Energy Sources, Part A* **2021**, *43*, 993−1006.
(3) Jiménez-García, J. C.; Ruiz, A.; Pacheco-Reyes, A.; Rivera, W. A Comprehensive Review of Organic Rankine Cycles. *Processes* **2023**, *11*, No. 1982, DOI: 10.3390/pr11071982.
(4) Ashwni; Sherwani, A. F.; Tiwari, D. Thermodynamic analysis of simple and modified organic Rankine cycle and vapor compression refrigeration (ORC-VCR) systems. *Environ. Prog. Sustainable Energy* **2021**, *40*, No. e13577.
(5) Goyal, A.; Sherwani, A. F.; Tiwari, D.; Kumar, A. Sensitivity analysis and multi-objective optimization of organic Rankine cycle integrated with vapor compression refrigeration system. *Energy Sources, Part A* **2025**, *47* (1), 7132−7144.
(6) Kargar, M. R.; Baniasadi, E.; Mosharaf-Dehkordi, M. Numerical analysis of a new thermal energy storage system using phase change materials for direct steam parabolic trough solar power plants. *Sol. Energy* **2018**, *170*, 594−605.
(7) Khatoon, S.; Almefreji, N. M. A.; Kim, M. H. Thermodynamic study of a combined power and refrigeration system for low-grade heat energy source. *Energies* **2021**, *14*, No. 410, DOI: 10.3390/en14020410.
(8) Kong, R.; Deethayat, T.; Asanakham, A.; Vorayos, N.; Kiatsiriroat, T. Thermodynamic performance analysis of a R245fa organic Rankine cycle (ORC) with different kinds of heat sources at evaporator. *Case Stud. Therm. Eng.* **2019**, *13*, No. 100385.
(9) Maali, R.; Khir, T. Performance analysis of different orc power plant configurations using solar and geothermal heat sources. *Int. J. Green Energy* **2020**, *17*, 349−362.
(10) Peyrovedin, H.; Haghbakhsh, R.; Duarte, A. R. C.; Shariati, A. Deep Eutectic Solvents as Phase Change Materials in Solar Thermal Power Plants: Energy and Exergy Analyses. *Molecules* **2022**, *27*, No. 1427, DOI: 10.3390/molecules27041427.
(11) Schilling, J.; Gross, J.; Bardow, A. Integrated design of ORC process and working fluid using process flowsheeting software and PC-SAFT. *Energy Procedia* **2017**, *129*, 129−136.
(12) Tchanche, B. F.; Papadakis, G.; Lambrinos, G.; Frangoudakis, A. Fluid selection for a low-temperature solar organic Rankine cycle. *Appl. Therm. Eng.* **2009**, *29*, 2468−2476.
(13) Bronicki, L. Y. *Organic Rankine Cycle (ORC) Power Systems: Technologies and Applications*; Elsevier Ltd, 2017; pp 25−66.
(14) Liu, B.-T.; Chien, K.-H.; Wang, C.-C. Effect of working fluids on organic Rankine cycle for waste heat recovery. *Energy* **2004**, *29*, 1207−1217.
(15) Chen, C.; Mu, H.; Li, N.; Zhao, X.; Song, Y.; Wang, H. Comparative Analysis of a Novel System Integrating ORC, Hydrogen Production, and Seawater Desalination with LNG Cold Energy: Energy, Economic, and Environmental Analyses. *Energy Fuels* **2023**, *37*, 16461−16475.
(16) Palma-Flores, O.; Flores-Tlacuahuac, A.; Canseco-Melchor, G. Optimal molecular design of working fluids for sustainable low-temperature energy recovery. *Comput. Chem. Eng.* **2015**, *72*, 334−349.
(17) Groniewsky, A.; Wagner, C. Investigation of the effect of the regenerative heat exchanger on the performance of organic Rankine cycles using perturbed chain−Statistical associating fluid theory equation of state. *Ind. Eng. Chem. Res.* **2020**, *59*, 19643−19656.
(18) Heberle, F.; Brüggemann, D. Exergy based fluid selection for a geothermal Organic Rankine Cycle for combined heat and power generation. *Appl. Therm. Eng.* **2010**, *30*, 1326−1332.
(19) European Parliament and Council. *Amendment to the Montreal Protocol on Substances That Deplete the Ozone Layer*, 2016.
(20) Intergovernmental Panel on Climate Change. *Climate Change 2007: Synthesis Report. Contribution of Working Groups I, II and III to the Fourth Assessment Report of the Intergovernmental Panel on Climate Change*, 2007; pp 75−104.
(21) Rhodes, C. J. The 2015 Paris climate change conference: COP21. *Sci. Prog.* **2016**, *99*, 97−104.
(22) Li, H.; Bu, X.; Wang, L.; Long, Z.; Lian, Y. Hydrocarbon working fluids for a Rankine cycle powered vapor compression refrigeration system using low-grade thermal energy. *Energy Build.* **2013**, *65*, 167−172.
(23) Imre, A. R.; Kustán, R.; Groniewsky, A. Thermodynamic Selection of the Optimal Working Fluid for Organic Rankine Cycles. *Energies* **2019**, *12*, No. 2028.
(24) Kolahi, M.; Yari, M.; Mahmoudi, S. M.; Mohammadkhani, F. Thermodynamic and economic performance improvement of ORCs through using zeotropic mixtures: Case of waste heat recovery in an offshore platform. *Case Stud. Therm. Eng.* **2016**, *8*, 51−70.
(25) Loni, R.; Najafi, G.; Bellos, E.; Rajaee, F.; Said, Z.; Mazlan, M. A review of industrial waste heat recovery system for power generation with Organic Rankine Cycle: Recent challenges and future outlook. *J. Cleaner Prod.* **2021**, *287*, No. 125070, DOI: 10.1016/j.jclepro.2020.125070.
(26) Mateu-Royo, C.; Mota-Babiloni, A.; Navarro-Esbrí, J.; Barragán-Cervera, Á. Comparative analysis of HFO-1234ze(E) and R-515B as low GWP alternatives to HFC-134a in moderately high temperature heat pumps. *Int. J. Refrig.* **2021**, *124*, 197−206.
(27) Vuppaladadiyam, A. K.; Antunes, E.; Vuppaladadiyam, S. S. V.; Baig, Z. T.; Subiantoro, A.; Lei, G.; Leu, S. Y.; Sarmah, A. K.; Duan, H. Progress in the development and use of refrigerants and unintended environmental consequences. *Sci. Total Environ.* **2022**, *823*, No. 153670.
(28) González, J.; Llovell, F.; Garrido, J. M.; Quinteros-Lama, H. A rigorous approach for characterising the limiting optimal efficiency of working fluids in organic Rankine cycles. *Energy* **2022**, *254*, No. 124191.
(29) González, J.; Garrido, J. M.; Quinteros-Lama, H. Analysis of the Maximum Efficiency and the Maximum Net Power as Objective Functions for Organic Rankine Cycles Optimization. *Entropy* **2023**, *25*, No. 882.
(30) González, J.; Llovell, F.; Garrido, J. M.; Quinteros-Lama, H. Selection of a suitable working fluid for a combined organic Rankine cycle coupled with compression refrigeration using molecular approaches. *Fluid Phase Equilib.* **2023**, *572*, No. 113847.
(31) González, J.; Llovell, F.; Garrido, J. M.; Quinteros-Lama, H. A study of the optimal conditions for organic Rankine cycles coupled with vapour compression refrigeration using a rigorous approach

https://doi.org/10.1021/acsomega.5c13210
ACS Omega 2026, 11, 22031−22043

based on the Helmholtz energy function. *Energy* **2023**, *285*, No. 129554.
(32) Qiu, K.; Entchev, E. A micro-CHP system with organic Rankine cycle using R1223zd(E) and n-Pentane as working fluids. *Energy* **2022**, *239*, No. 121826.
(33) Albà, C. G.; Alkhatib, I. I. I.; Vega, L. F.; Llovell, F. Mapping the Flammability Space of Sustainable Refrigerant Mixtures through an Artificial Neural Network Based on Molecular Descriptors. *ACS Sustainable Chem. Eng.* **2024**, *12*, 11561−11577.
(34) Zhao, S.; Abed, A. M.; Deifalla, A.; Al-Zahrani, A.; Aryanfar, Y.; Alcaraz, J. L. G.; Galal, A. M.; Sai, W. Competitive study of a geothermal heat pump equipped with an intermediate economizer for various ORC working fluids. *Case Stud. Therm. Eng.* **2023**, *45*, No. 102954.
(35) Shu, G.; Zhao, M.; Tian, H.; Wei, H.; Liang, X.; Huo, Y.; Zhu, W. Experimental investigation on thermal OS/ORC (Oil Storage/Organic Rankine Cycle) system for waste heat recovery from diesel engine. *Energy* **2016**, *107*, 693−706.
(36) Birriel, A.; Romero, J.; Saavedra, N.; Quinteros-Lama, H.; González, J. Thermal and Exergetic Performance Assessment of an ORC Coupled with Thermal Energy Storage Using Thermal Oils for Low-Grade Heat Recovery. *Appl. Sci.* **2025**, *15*, No. 6153, DOI: 10.3390/app15116153.
(37) Dragomir-Stanciu, D.; Luca, C. Solar Power Generation System with Low Temperature Heat Storage. *Procedia Technol.* **2016**, *22*, 848−853.
(38) Nazir, H.; Batool, M.; Osorio, F. J. B.; Isaza-Ruiz, M.; Xu, X.; Vignarooban, K.; Phelan, P.; Inamuddin; Kannan, A. M. Recent developments in phase change materials for energy storage applications: A review. *Int. J. Heat Mass Transfer* **2019**, *129*, 491−523.
(39) Fang, G.; Yu, M.; Meng, K.; Shang, F.; Tan, X. High-Performance Phase-Change Materials Based on Paraffin and Expanded Graphite for Solar Thermal Energy Storage. *Energy Fuels* **2020**, *34*, 10109−10119.
(40) Gutiérrez-Blandón, C.; Cuadri, A. A.; Delgado-Sánchez, C.; Partal, P.; Navarro, F. J. Study on Miscibility, Thermomechanical Behavior, and Thermoregulation Performance of Paraffin Wax/Bituminous Blends for Solar Thermal Energy Storage Applications. *Energy Fuels* **2024**, *38*, 3407−3416.
(41) Ukrainczyk, N.; Kurajica, S.; Šipušić, J. Thermophysical comparison of five commercial paraffin waxes as latent heat storage materials. *Chem. Biochem. Eng. Q.* **2010**, *24*, 129−137.
(42) Daniarta, S.; Kolasiński, P.; Imre, A. R. Performance map and theoretical analysis of Carnot battery technology via novel reversible Rankine-based cycle. *Energy Rep.* **2024**, *11*, 4500−4514.
(43) Kolasiński, P. Experimental and modelling studies on the possible application of heat storage devices for powering the ORC (organic rankine cycle) systems. *Therm. Sci. Eng. Prog.* **2020**, *19*, No. 100586.
(44) Daniarta, S.; Kolasiński, P.; Imre, A. R. A Preliminary Design and Modeling Analysis of Two-Phase Volumetric Expanders for a Novel Reversible Organic Rankine-Based Cycle for Carnot Battery Technology. *Appl. Sci.* **2022**, *12*, No. 3557, DOI: 10.3390/app12073557.
(45) Daniarta, S.; Nemś, M.; Kolasiński, P.; Pomorski, M. Sizing the Thermal Energy Storage Device Utilizing Phase Change Material (PCM) for Low-Temperature Organic Rankine Cycle Systems Employing Selected Hydrocarbons. *Energies* **2022**, *15*, No. 956, DOI: 10.3390/en15030956.
(46) Daniarta, S.; Nemś, M.; Kolasiński, P. A review on thermal energy storage applicable for low- and medium-temperature organic Rankine cycle. *Energy* **2023**, *278*, No. 127931.
(47) Ali, S. A.; Habib, K.; Younas, M.; Rahman, S.; Das, L.; Rubbi, F.; Mulk, W. U.; Rezakazemi, M. Advancements in Thermal Energy Storage: A Review of Material Innovations and Strategic Approaches for Phase Change Materials. *Energy Fuels* **2024**, *38*, 19336−19392.
(48) Matuszek, K.; Vijayaraghavan, R.; Kar, M.; Macfarlane, D. R. Role of Hydrogen Bonding in Phase Change Materials. *Cryst. Growth Des.* **2020**, *20*, 1285−1291.
(49) Abbott, A. P.; Boothby, D.; Capper, G.; Davies, D. L.; Rasheed, R. K. Deep Eutectic Solvents formed between choline chloride and carboxylic acids: Versatile alternatives to ionic liquids. *J. Am. Chem. Soc.* **2004**, *126*, 9142−9147.
(50) Zhang, Q.; Vigier, K. D. O.; Royer, S.; Jérôme, F. Deep eutectic solvents: Syntheses, properties and applications. *Chem. Soc. Rev.* **2012**, *41*, 7108−7146.
(51) Alencar, L.; González-Barramuño, B.; Rodriguez-Reartes, S.; Quinteros-Lama, H.; Garrido, J.; Codera, V.; Pou, J.; Tavares, F.; Gonzalez-Olmos, R.; Llovell, F. Thermophysical Characterization of Sustainable Pathways for Hydrofluorocarbons Separation Utilizing Deep Eutectic Solvents. *J. Ind. Eng. Chem.* **2024**, *146*, 788−799, DOI: 10.1016/j.jiec.2024.12.005.
(52) Imas, C.; González, J.; Llovell, F.; Garrido, J. M.; Quinteros-Lama, H. Deep eutectic solvents and traditional refrigerants in absorption refrigeration cycles using molecular approaches. *Energy* **2024**, *308*, No. 133048.
(53) Maugeri, Z.; De María, P. D. Novel choline-chloride-based deep-eutectic-solvents with renewable hydrogen bond donors: Levulinic acid and sugar-based polyols. *RSC Adv.* **2012**, *2*, 421−425.
(54) Alvi, J. Z.; Feng, Y.; Wang, Q.; Imran, M.; Pei, G. Effect of phase change materials on the performance of direct vapor generation solar organic Rankine cycle system. *Energy* **2021**, *223*, No. 120006.
(55) Alvi, J. Z.; Feng, Y.; Wang, Q.; Imran, M.; Alvi, J. Modelling, simulation and comparison of phase change material storage based direct and indirect solar organic Rankine cycle systems. *Appl. Therm. Eng.* **2020**, *170*, No. 114780.
(56) Iasiello, M.; Braimakis, K.; Andreozzi, A.; Karellas, S. Thermal analysis of a Phase Change Material for a Solar Organic Rankine Cycle. *J. Phys.: Conf. Ser.* **2017**, *923*, No. 012042.
(57) Yekoladio, P. J.; Bello-Ochende, T.; Meyer, J. P. Thermodynamic analysis and performance optimization of organic rankine cycles for the conversion of low-to-moderate grade geothermal heat. *Int. J. Energy Res.* **2015**, *39*, 1256−1271.
(58) Keenan, J.; Chao, J.; Kaye, J. *Gas Tables: Thermodynamic Properties of Air Products of Combustion and Component Gases, Compressible Flow Functions*; Wiley, 1980.
(59) Kumar, S.; Nautiyal, S. P.; Khan, H. U.; Agrawal, K. M.; Dimri, J. K. Composition and Properties of Some Petroleum Waxes. *Pet. Sci. Technol.* **2005**, *23*, 939−951.
(60) Zhao, B. Y.; Xu, P.; Yang, F. X.; Wu, H.; Zong, M. H.; Lou, W. Y. Biocompatible Deep Eutectic Solvents Based on Choline Chloride: Characterization and Application to the Extraction of Rutin from Sophora japonica. *ACS Sustainable Chem. Eng.* **2015**, *3*, 2746−2755.
(61) Pyykkö, P. Simple Estimates for Eutectic Behavior. *ChemPhysChem* **2019**, *20*, 123−127.
(62) Joback, K. G.; Reid, R. C. Estimation of Pure-Component Properties from Group-Contributions. *Chem. Eng. Commun.* **1987**, *57*, 233−243.
(63) López-Porfiri, P.; Brennecke, J. F.; Gonzalez-Miquel, M. Excess molar enthalpies of deep eutectic solvents (DESs) composed of quaternary ammonium salts and glycerol or ethylene glycol. *J. Chem. Eng. Data* **2016**, *61*, 4245−4251.
(64) López-Porfiri, P.; Brennecke, J. F.; Gonzalez-Miquel, M. Excess Molar Enthalpies of Deep Eutectic Solvents (DESs) Composed of Quaternary Ammonium Salts and Glycerol or Ethylene Glycol. *J. Chem. Eng. Data* **2016**, *61*, 4245−4251.
(65) Maugeri, Z.; de María, P. D. Novel choline-chloride-based deep-eutectic-solvents with renewable hydrogen bond donors: levulinic acid and sugar-based polyols. *RSC Adv.* **2012**, *2*, 421−425.
(66) Siddiqui, M. U.; Owes, A.; Al-Amri, F. G.; Saeed, F. Recent developments in the search for alternative low-global-warming-potential refrigerants: A review. *Int. J. Air-Cond. Refrig.* **2020**, *28*, No. 2030004, DOI: 10.1142/S2010132520300049.
(67) Shaik, S. V.; Babu, T. P. Theoretical Performance Investigation of Vapour Compression Refrigeration System Using HFC and HC Refrigerant Mixtures as Alternatives to Replace R22. *Energy Procedia* **2017**, *109*, 235−242.

(68) Alao, J. O.; Saqr, A. M.; Ayejoto, D. A.; Otorkpa, O. J.; Abubakar, F.; Mohammed, M. A.; Ibe, A. A. Environmental impacts of hydrocarbon contaminants and associated potential public health risks. *J. Hazard. Mater.* **2025**, *19*, No. 100853.
(69) Ata, S. I.; Kahraman, A.; Sahin, R. Prediction and sensitivity analysis under different performance indices of R1234ze ORC with Taguchi's multi-objective optimization. *Case Stud. Therm. Eng.* **2020**, *22*, No. 100785.
(70) Garavagno, M. D. l. A.; Wenger, A.; Holland, R. E. T.; Fena, B. R.; Goldstein, S. D.; Hicks, D. E.; Liu, F.; Madell, J. B.; Solomon, S. J.; Kuwata, K. T.; McGillen, M. R.; Khan, M. A. H.; Shallcross, D. E.; Stanley, K. M.; Orr-Ewing, A. J. Atmospheric Oxidation of Hydrofluoroolefins and Hydrochlorofluoroolefins by Ozone Produces HFC-23, PFC-14, and CFC-13. *Environ. Sci. Technol.* **2025**, *59*, 26031−26040.
(71) Gross, J.; Sadowski, G. Perturbed-Chain SAFT: An equation of state based on a perturbation theory for chain molecules. *Ind. Eng. Chem. Res.* **2001**, *40*, 1244−1260.
(72) Fouad, W. A. Thermal Conductivity of Pure Fluids and Multicomponent Mixtures Using Residual Entropy Scaling with PC-SAFT−Application to Refrigerant Blends. *J. Chem. Eng. Data* **2020**, *65*, 5688−5697.
(73) González, J.; Llovell, F.; Garrido, J. M.; Quinteros-Lama, H. Accurate and Model-Free Control Function for a Single Stage Transcritical Refrigerator Cycle. *ACS Omega* **2020**, *5*, 19217−19226.
(74) Mimoune, Z.; Anoune, I.; Madani, H. Implementation of PC-SAFT for Predicting thermodynamic properties of pure refrigerants and vapor-liquid equilibria of refrigerants binary mixtures. *Fluid Phase Equilib.* **2023**, *573*, No. 113868.
(75) Wang, J.; Chen, D.; Zhu, L. Integrated Working Fluids and Process Optimization for Refrigeration Systems Using Polar PC-SAFT. *Ind. Eng. Chem. Res.* **2021**, *60*, 17640−17649.
(76) Vinš, V.; Hrubý, J. Solubility of nitrogen in one-component refrigerants: Prediction by PC-SAFT EoS and a correlation of Henry's law constants. *Int. J. Refrig.* **2011**, *34*, 2109−2117.
(77) Raabe, G. Molecular Simulation Studies on the Vapor-Liquid Phase Equilibria of Binary Mixtures of R-1234yf and R-1234ze(E) with R-32 and CO_2. *J. Chem. Eng. Data* **2013**, *58*, 1867−1873.
(78) Groniewsky, A.; Wagner, C. Investigation of the effect of the regenerative heat exchanger on the performance of organic Rankine cycles using perturbed chain Statistical associating fluid theory equation of state. *Ind. Eng. Chem. Res.* **2020**, *59*, 19643−19656.
(79) Sun, W.; Yue, X.; Wang, Y. Exergy efficiency analysis of ORC (Organic Rankine Cycle) and ORC-based combined cycles driven by low-temperature waste heat. *Energy Convers. Manage.* **2017**, *135*, 63−73.

https://doi.org/10.1021/acsomega.5c13210
ACS Omega 2026, 11, 22031−22043